IVYSPRING INTERNATIONAL PUBLISHER

Nanotheranostics

2018; 2(1): 59-69. doi: 10.7150/ntno.22754

Research Paper

Oxygen Self-Sufficient Amphiphilic Polypeptide Nanoparticles Encapsulating BODIPY for Potential Near Infrared Imaging-guided Photodynamic Therapy at Low Energy

Le Liu, Zheng Ruan, Pan Yuan, Tuanwei Li, and Lifeng Yan ✉

CAS Key Laboratory of Soft Matter Chemistry, Department of Chemical Physics, iCHEM, University of Science and Technology of China. Hefei, 230036, P.R. China.

✉ Corresponding author: Lifeng Yan, Fax: +86-551-63603748; Tel: +86-551-63606853; E-mail: lfyan@ustc.edu.cn

Received: 2017.09.08; Accepted: 2017.11.10; Published: 2018.01.01

Abstract

Near infrared (NIR) imaging-guided photodynamic therapy (PDT) is remarkable for its high-efficiency in "see and treat" field. However, hypoxia of cancer cell limits PDT dues to the low singlet oxygen yield. Here MnO_2 conjugated multifunctional polypeptide nanoparticles encapsulating photosensitizer BODIPY has been prepared via a one-step reaction, which can generate oxygen in cancer cytoplasm where rich of H_2O_2, following singlet oxygen by photosensitizer under NIR light irradiation. *In vitro* studies on HepG2 and 4T1 cancer cells revealed that the as-prepared nanoparticles obviously increase the cell suppression rate under hypoxia conditions, even exposed to an extremely low light energy density (25 mW/cm^2). Meanwhile, excellent NIR fluorescence property of BODIPY enabled the nanoparticles to light up the cancer cells for real-time imaging. These results suggest the promises of biocompatible and biodegradable nanoparticles has potential application on efficient NIR imaging-guided photodynamic therapy.

Key words: polypeptide nanoparticles, photodynamic therapy (PDT), near-infrared fluorescence (NIRF), imaging-guided, hypoxia

Introduction

Photodynamic therapy (PDT), which kills cancer cells by reactive oxygen species (ROS) when photosensitizers (PSs) were exposed to light in the presence of oxygen, has attracted increasing attention in recent years.[1-3] To achieve imaging-guided PDT, excellent PSs needs to have both high near-infrared (NIR) emission and singlet oxygen ($^1O_2$) generation efficiency,[4, 5] among which heavy atoms modified 4, 4-difluoro-4-bora-3a, a-diaza-s-indacene (BODIPY) PSs have been widely studied.[6, 7]

However, most of the existing BODIPY PSs are usually too hydrophobic to be delivered to the tumor tissues. To solve this problem, a variety of nanomaterials (liposomes, polymers, quantum dots, metallic nanostructures, etc.) have been designed,[8-11] among which amphiphilic polymer nanoparticles have been proved effective in protecting PSs from water invasion.[12-14] Besides, the well-designed compositions, sizes, morphologies make polymer-PS NPs easily accumulate in the tumor tissue through enhanced permeability and retention (EPR) effect, and then present effective PDT under light irradiation.[15]

Oxygen is necessary for PDT for the efficient generation of singlet oxygen. Unfortunately, hypoxia is a common characteristic of the tumor microenvironment (TME) resulting from the rapid growth of cancer cells.[16] Moreover, oxygen consumption to $^1O_2$ during PDT can aggravate the insufficient oxygen supply, which will in turn

hampers PDT from achieving its full photodynamic efficacy.[17, 18] Various strategies have been explored to overcome this problem, including dividing irradiation into dark-light circles to affect PDT-induced oxygen depletion, transport oxygen to tumor tissues with artificial blood substitutes, and in situ oxygen generation with catalysts inside tumors.[19-21] Since manganese dioxide (MnO_2) shows high reactivity toward H_2O_2 to produce O_2, it is predicted to supply O_2 to tumor microenvironment or inside cancer cell since the concentration of H_2O_2 is higher therein.[22] More importantly, the reaction between MnO_2 and H_2O_2 under acidic pH, which is not purely catalytic, can consume MnO_2 to break down to harmless Mn^{2+} ions. These characteristics could be particularly favorable for biological applications with less accumulating toxicity in the body.

Envisioning the effectiveness of the MnO_2-catalyzed H_2O_2 decomposition to produce O_2 to overcome the hypoxia situation in PDT, we have developed biocompatible MnO_2 and BODIPY loaded NPs (PMB NPs) and verified their multifunctionality in eliminating hypoxia and then high-efficiently killing cancer cells with light irradiation. Polypeptides were chose in our study for their biocompatibility and biodegradability,[23] and easy preparation via ring-opening polymerization of N-carboxyanhydrides monomer (NCA). So firstly, an amino-functionalized copolymer (POEGMA-PLys) was prepared, in which POEGMA worked for its stabilization in aqueous environment. Then after the loading of MnO_2 and BODIPY, the as-prepared polymer-MnO_2-BODIPY (PMB NPs) were demonstrated to possess the following abilities: (1) remitting hypoxia via reaction of MnO_2 towards H_2O_2 to generate amounts of O_2 in situ, (2) increasing pH by consuming protons during the above reaction, (3) tracing cancer cells relying on the high fluorescence emission of BODIPY, and (4) suppressing cancer cells growth in the presence of H_2O_2 and light under hypoxia condition. Taken together, oxygen self-sufficient nanoparticles carrying BODIPY for simultaneous low energy triggered imaging and treating has been prepared.

Experimental Section

Materials

Organic solvents were purchased from Sinoreagent Corporation. N, N-dimethyl formamide (DMF), tetrahydrofunan (THF), dichloromethane (DCM) and n-hexane were dried over CaH_2 before use. All reagents in AR purity were purchased from Aladdin Corporation (China) and used without further purification. Oligo (ethylene glycol) methacrylate (OEGMA) was purified using silica gel before immediate polymerization. Dulbecco modified eagle medium (DMEM), fetal bovine serum (FBS), fluorescein diacetate (FDA), propidium iodide (PI), 4′,6-diamidino-2-phenylindole (DAPI) and methyl thiazolyl tetrazolium (MTT) were purchased from Sangon Corporation (China). A Milli-Q (18.2 MΩ) Synthesis System (Millipore, Bedford, MA, USA) was used to prepare ultrapure water. Dialysis bags (cut off M_w=7000 or 1000) were obtained from Bomei Biotechnology Corporation (China).

Characterization

^{1}H-NMR spectra, using either DMSO-$_{d6}$ or $CDCl_3$ containing 0.03% (v/v) TMS as solvent, were measured on a Bruker AC 300 NMR spectrometer. UV-Vis spectra were measured on a Shimadzu UV-2401 PC Ultraviolet while fluorescence spectra were recorded on Shimadzu RF-5301PC. FT-IR spectra, applying a KBr method, were recorded on a Bruker EQUINOX 55 spectrometer. The molecular weights of the prepared samples (5mg/mL) were determined with gel permeation chromatography (GPC, KD-804 column and RID-10A refractive index detector), using DMF as the mobile phase at 60 ^{o}C. Raman spectra were recorded on a Bruker spectromet er with a 532nm laser. Dynamic light scattering (DLS) were measured via a Malvern Zetasizer Nano ZS90. JEOL-2010 microscope was used to obtain transmission electron microscopy (TEM) images. The fluorescence microscope imaging experiments were conducted on an Olympus U-HGLGPS fluorescence microscope. A Bio-rad iMark microplate reader was applied to record the MTT absorbance. The dissolved oxygen is estimated by a dissolved oxygen meter AZ 8403 at room temperature.

Methods

Synthesis of $POEGMA_{30}$ (1)

RAFT-APA (230mg, 0.474 mmol), OEGMA (11.8g, 23.7 mmol, 50 equiv) and AIBN (13.5mg, 0.118 mmol, 1/4 equiv) were dissolved in DMF (5 mL) into a flame dried and argon purged Schlenk tube and stirred at 80 °C for 12 h. After cooling to room temperature, the solution was purified by dialysis using ultrapure water and freeze dried to obtain a yellow viscous liquid (6.42g, 90.3%). (Figure S5)

Synthesis of $PLys_{10}$ (2)

Firstly, Nε-Carbobenzoxy-L-lysine (2.74g, 9.82 mmol) and triphosgene (3.19g, 10.8 mmol, 1.1 equiv) was mixed in dry DMF (40 mL) under a nitrogen atmosphere and stirred at 45 °C for 2 h. After cooling in an ice-water bath, crystallized with dried hexane

and THF, white solid Lys-NCA was obtained and was dried over a vacuum line for 4 h.

Then propargylamine (35.8mg, 0.650 mmol) was solubilized in dry DMF (10 mL) into a flame dried and argon purged Schlenk tube. And Lys-NCA (1.99g, 6.50 mmol, 10 equiv) in dry DMF (8mL) was added at 0 °C and kept stirring for 3 days. After stirring at room temperature overnight, the solution was purified by dialysis with ultrapure water and freeze dried to get a white solid (1.75g, 92.0%). (Figure S5)

Synthesis of $POEGMA_{30}$-$PLys_{10}$ (3)

To a flame dried and argon purged Schlenk tube, **2** (915mg, 61.0 μmol) and **3** (164mg, 61.0 μmol) were dissolved in DMF (10mL), and then CuBr (8.9mg, 61.0 μmol) and PMDETA (10.5mg, 61.0 μmol) was added to give a click reaction at 30 °C for 3 days. The solution was purified by dialysis with EDTA added ultrapure water and freeze dried to obtain a yellow solid (671mg, 83.5%).

Amino Deprotection of Polymer 3 (4)

Polymer **3** (350mg, 1.97 μmol) was dissolved in trifluoroacetic acid (5mL) and HBr–acetic acid (33 wt%, 500 μL) was then added in an ice-water bath. After stirring for 5 h at room temperature, the solution was precipitated and washed with excess diethyl ether to get a sticky yellow solid (302mg, 92.2%).

Preparation of Polymer-MnO_2 Nanoparticles (PM NPs)

PM NPs were prepared by directly mixing the aqueous solutions of amino-contained polymer **4** and $KMnO_4$. Briefly, 100 μL of $KMnO_4$ solution (14.3 mg/mL) was added into 5 mL of polymer (30mg) solution, and the mixture was stirred for 20 min at room temperature. The conversion of permanganate to MnO_2 was confirmed by recording UV-vis absorption spectrum. Finally a filter membrane (450nm) was applied to remove the unstable particles.

Preparation of Polymer-MnO_2-BODIPY Nanoparticles (PMB NPs)

PMB NPs were prepared by emulsion-volatilization method. In brief, 5mL of the as-prepared PM NPs solution and 0.3mL BODIPY (5mg) in CH_2Cl_2 were mixed to get emulsion with ultrasonic treatment. Then CH_2Cl_2 was removed by volatilization and a filter membrance (450nm) was applied to remove the unstable particles.

Detection of Singlet Oxygen.

Singlet oxygen generation of PMB NPs was detected using a 635 lamp at 25 mW/cm^2. PMB NPs and DPBF were dissolved in 2% DMSO contained deionized water and irradiated with light. The absorbance of the solution was measured at every predetermined time points. The absorbance reduction of DPBF was considered to quantify the $^1O_2$ generation efficiency.

Cell Lines and Cytocompatibility

Human HepG2 and murine 4T1 cells obtained from American Type Culture Collection were incubated in DMEM or 1640 medium respectively (containing 10% FBS) at 37 °C under 5% CO_2 atmosphere.

The cytocompatibility of PMB NPs over HepG2 and 4T1 cells was conducted using a standard MTT assay. In brief, HepG2 or 4T1 cells (3000 cells per well) were seeded onto 96-well plates and allowed to incubate for 24 h. Fresh medium with PMB NPs (0-0.3 mg/mL) were added and incubated for 8 h. After medium was changed incubated overnight, MTT was added and incubated for 4h. The absorbance of cell lysate in DMSO (150 μL) was measured at 570nm.

Cellular Uptake of NPs.

HepG2 and 4T1 tumor cells (10^5cells per well) were plated onto 6-well plates and incubated for 24 h. Then fresh medium with PMB NPs (0.3 mg/mL) was added and incubated for a scheduled time. After fixed with 4% formaldehyde, cell nuclei were stained blue with DAPI (100 ng/mL) and observed through a fluorescence microscope.

In Vitro Photodynamic Therapy and Cell Apoptosis

For photodynamic therapy experiments, HepG2 or 4T1 cells (3000 cells per well) were seeded onto 96-well plates and incubated for 24 h. Then fresh medium with PMB or PB NPs (0-0.3mg/mL) were added and incubated for 8 h under normal or N_2 atmosphere. After irradiated for 10 min (635nm, 25 mW/cm^2) or not, medium was changed and cells were incubated overnight. A standard MTT protocol was used to measure cell viability. Experimental groups with H_2O_2 (100 μM) added 4 h before irradiation was also conducted.

Observable laser-induced PDT effect was presented by staining experiments of live or dead cells. HepG2 and 4T1 tumor cells (10^5 cells per well) were plated onto 6-well plates and incubated for 24 h. Then fresh medium with PMB or PB NPs (0.3 mg/mL) was added and incubated for 8 h under normal or hypoxia (N_2) atmosphere. After 10 min irradiation (635nm, 25 mW/cm^2) or not, medium was changed and the cells were allowed to incubate overnight. Then live or dead cells were stained with FDA (10 μg/mL) or PI (100 μg/mL) respectively for 15 min at 37 °C, and observed through a fluorescence microscope. Experimental groups with H_2O_2 (100 μM) added 4 h before irradiation was also conducted.

Cell apoptosis experiments were conducted applying cell nuclei staining assay using DAPI against HepG2 tumor cells (10^5cells per well). After plated and incubated for 24 h, cells were cultured with fresh medium with PMB or PB NPs (BODIPY 10μM) for another 12h and then exposed to light (635nm, 25 mW/cm^2) or not. After fixed with 4% formaldehyde, cell nuclei were stained blue with DAPI (100 ng/mL) and observed through a fluorescence microscope for a scheduled time.

Results and Discussion

Preparation of PMB NPs

To efficiently load MnO_2 and deliver PSs, we designed an amphiphilic block polymer, in which poly-oligo (ethylene glycol) methacrylate (POEGMA) worked as a hydrophilic shell, and peptides as a hydrophobic core. As shown in Scheme 1, an azido modified RAFT agent was firstly prepared according to our previous work,[24] and then used to RAFT-polymerize OEGMA (PDI=1.17, Table 1). Meanwhile, ring-opening polymerization (ROP) of Lys-NCA was conducted applying propargylamine as the initiator to obtain $PLys_{10}$ (PDI=1.14). After the click reaction of these two segments, the copolymer was exposed to HBr to carry out amino deprotection for the latter reduction reaction of manganese permanganate. Completion of click reaction could be proved by the disappearance of 2063 cm^{-1} peak of N_3 in FT-IR spectra (Figure S1) and the increase in molecular weight of the polymer (Figure S2). The disappearance of benzene peaks in ^{1}H-NMR spectra proved the preparation of amino-contained copolymer. As shown in Figure 1, after the amino deprotection of copolymer, the peaks of benzyl groups disappeared (4.98ppm and 7.30ppm) while the chemical shift of protons m slightly moved to a higher field (from 2.94ppm to 2.78ppm).

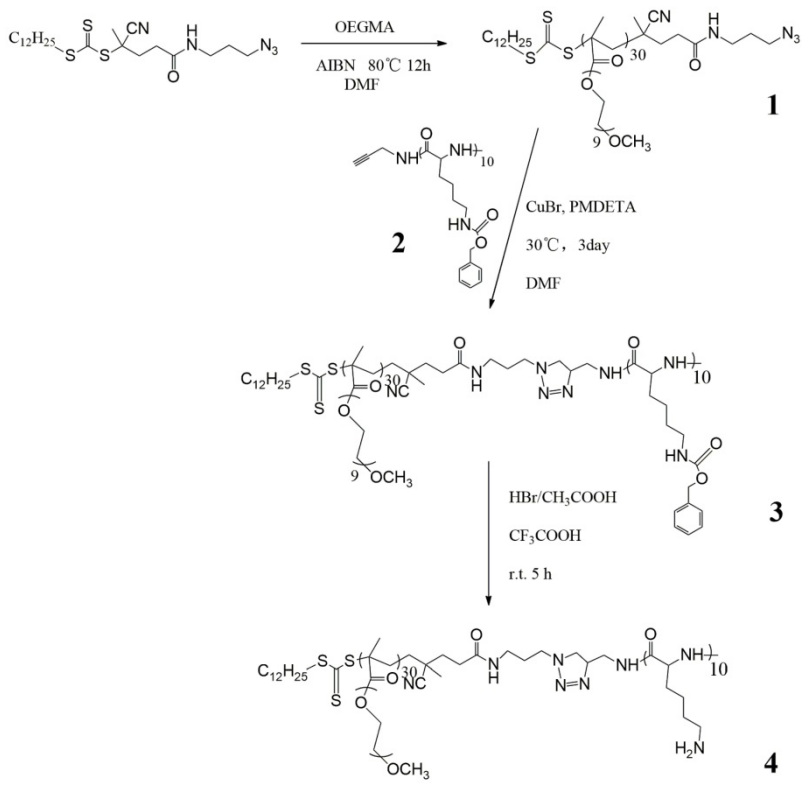

Scheme 1. Synthesis of the amino-contained amphiphilic copolymer.

Table 1. Molecular weights and polydispersity indexes of the obtained copolymers.

Sample	M_n^{NMR}	M_n^{GPC}	PDI
$PLys_{10}$	2675	2760	1.14
$POEGMA_{30}$	15485	16725	1.17
$POEGMA_{30}$-$PLys_{10}$	19400	21240	1.12
$POEGMA_{30}$-$PLys(NH_2)_{10}$	17030	-	-

It has been reported that $KMnO_4$ could be reduced to MnO_2 by organic amine compounds,[25, 26] so we employed a one-step method using the as-prepared amino-involved polymer to reduce $KMnO_4$ to get polymer-MnO_2 (PM NPs) in 20 min, as shown in Figure 2a. The solution color would gradually change from purple to brown, until the UV-vis absorption peak of $KMnO_4$ disappeared. Peaks at 507, 571, 646 cm^{-1} in the Raman spectrum (Figure 2b) of PMB confirmed the generation of γ-MnO_2.[27] XRD spectrum of the PMB nanoparticles in Figure 2c shows four broad diffraction peaks at 24.4 °, 37.7 °, 52.6 ° and 65.9 °. Meanwhile XPS spectra of PMB NPs could be roughly detected, and in the Mn 2p pattern, two main peaks located at 654.1 eV (Mn 2p1/2) and 642.6 eV (Mn 2p2/3) with a spin-energy separation of 11.6 eV.[28] The broad peaks in XRD and weak signals in XPS all revealed the poor crystallization of PMB mainly caused by the coverage of polymers on the surface of MnO_2. The polymer used here served as not only a reducing reagent, but also a protective layer to stabilize the as-formed NPs. This procedure was rapid and gave stable PM dispersions with an average size distribution of 50.8nm (Figure 3a, 3c).

It was reported that heavy atoms modified BODIPY dyes displayed outstanding properties, such as high NIR absorbance and fluorescence emission, especially their massive singlet oxygen generation.[29] So an excellent BODIPY dye was synthesized according to our precious work (Scheme S1), and it shows

a λ_{max} = 721nm with λ_{em} = 788nm, ϕ_{Δ} ($^1O_2$) = 0.36 in $CHCl_3$ (Figure S3).[30] The BODIPY molecules were encapsulated into PMB NPs by an emulsion method for efficient NIR imaging and PDT. It could be effectively introduced to the core of NPs by the hydrophobic interaction between MnO_2 and BODIPY, and the photosensitizer loading content (PLC) was calculated to be about 3.2% applying the following equation, as measured by UV–vis absorbance spectra.

$$\text{PLC (wt \%)} = \left(\frac{weight\ of\ loaded\ photosensitizer}{weight\ of\ NPs}\right) \times 100\%$$

When BODIPY dye is added to the reaction mixture, the nanoparticles turned much bigger mainly caused by the severe hydrophobicity of BODIPY, leading to a further aggregation of NPs core. DLS showed PMB NPs had an average sizes distribution of 169.2nm (Figure 3b), and the Zeta potential was +14.5mV due to the existence of MnO_2, which could befit the NPs enter the tumor cells. TEM images were accordant with the DLS results, and further revealed their nano-size and spherical shape (Figure 3d).

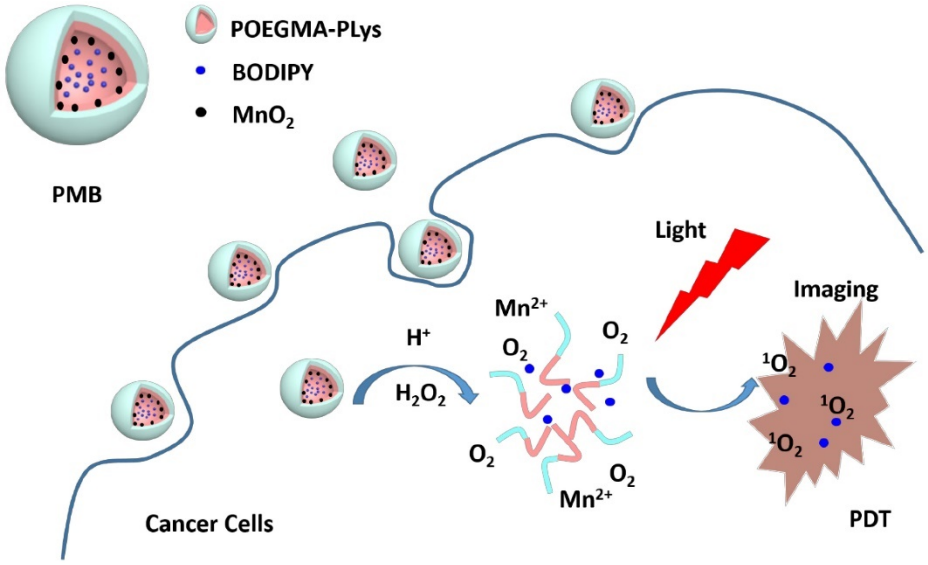

Scheme 2. PMB NPs reacting with endogenous H_2O_2, NIR imaging and photodynamic therapy on cancer cells.

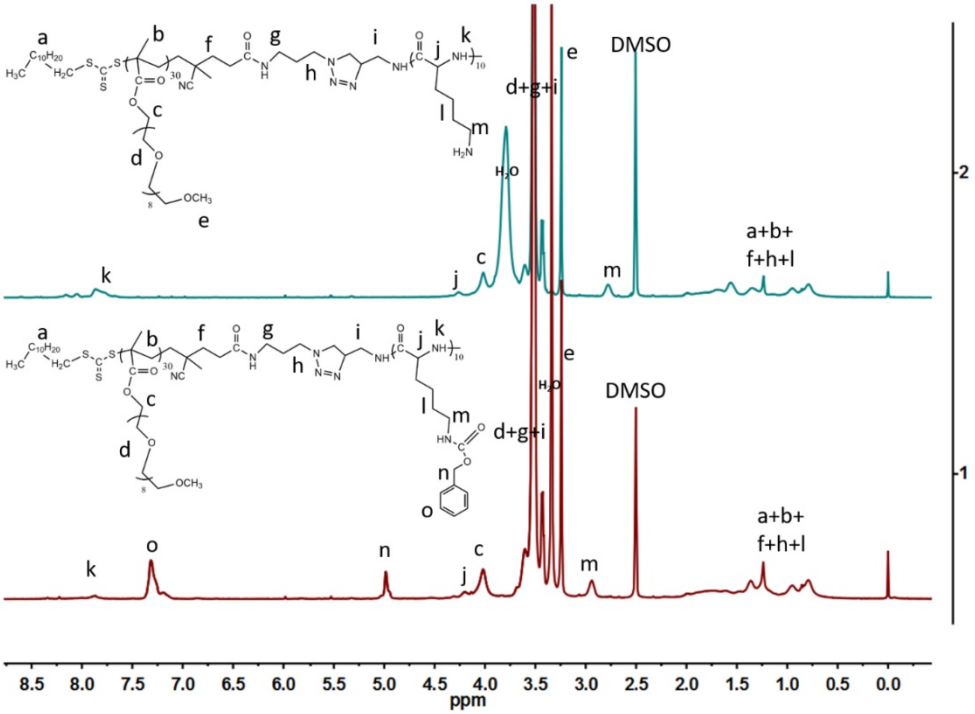

Figure 1. ^{1}H-NMR spectra comparison of (1) $POEGMA_{30}$-$PLys_{10}$ and (2) $POEGMA_{30}$-PLys $(NH_2)_{10}$.

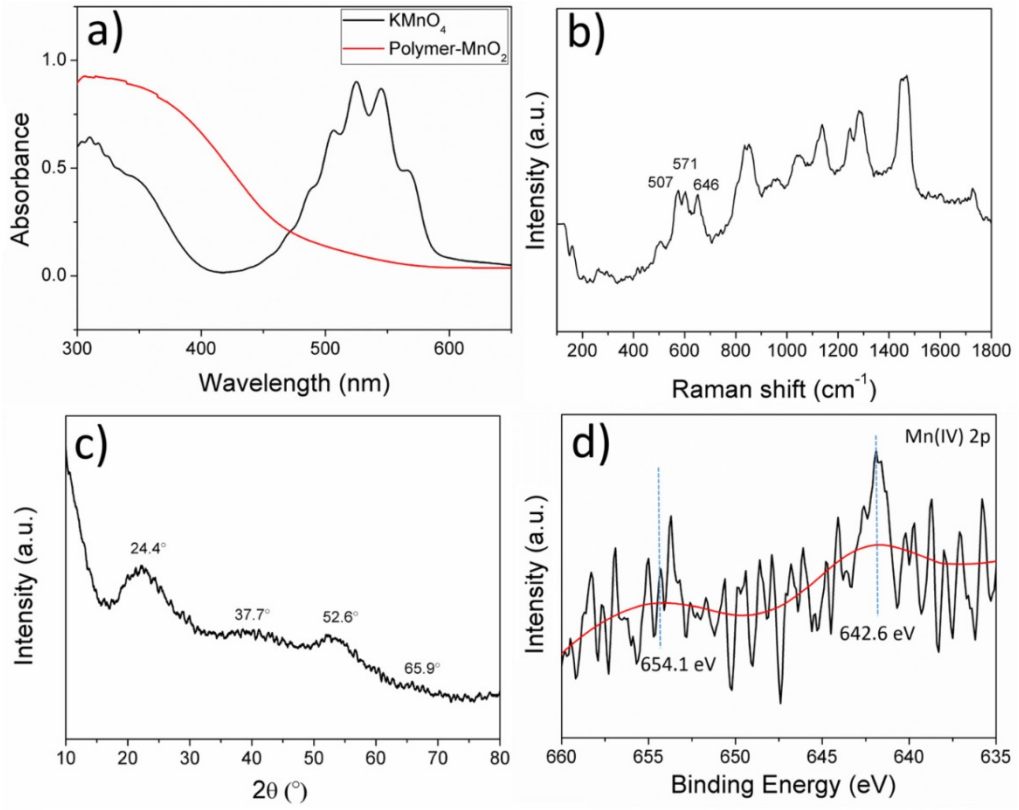

Figure 2. (a) UV-vis absorption spectra of $KMnO_4$ and PM NPs in deionized water solutions at room temperature; (b) Raman spectrum of PMB NPs; (c) XRD spectrum of PMB NPs and (d) XPS spectrum of PMB NPs.

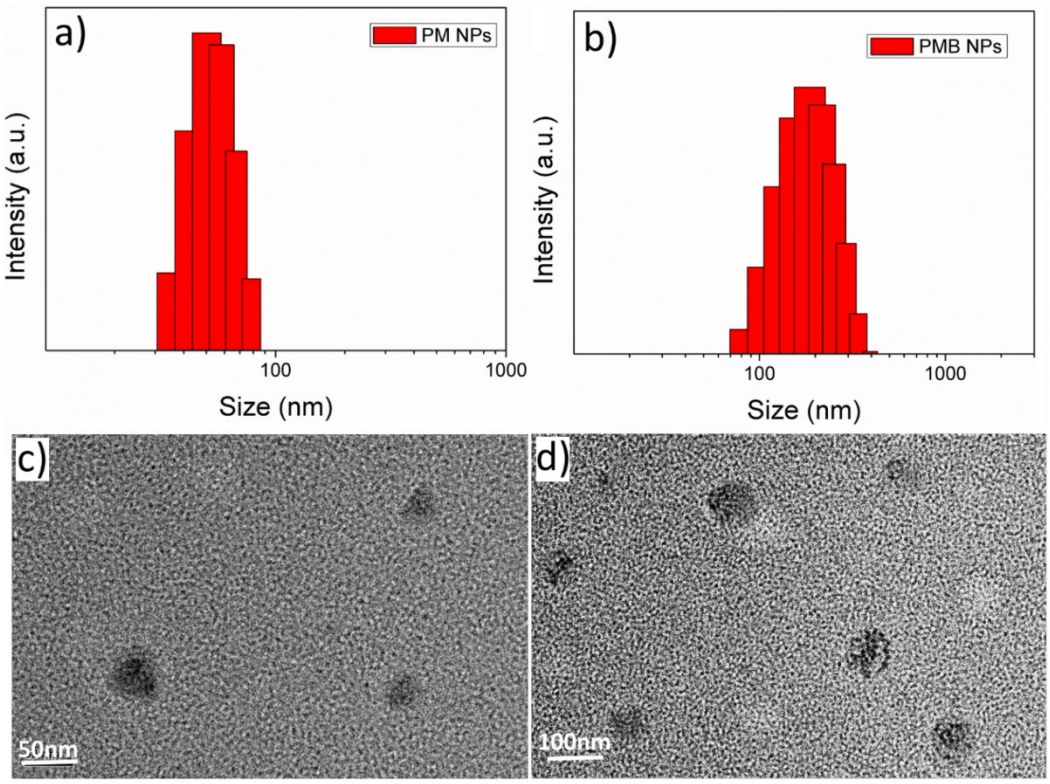

Figure 3. Size distribution of (a) PM NPs and (b) PMB NPs; TEM image of (c) PM NPs and (d) PMB NPs.

Oxygen Generation and Singlet Oxygen Detection

Upon reaction with H_2O_2 at an endogenous level,[31] we first investigated the functionality of PM NPs to generate O_2. Reaction between MnO_2 and H_2O_2, which is summarized in Figure 4a, is a complex reaction to produce O_2 by the consumption of H^+ ions and decomposition of H_2O_2. In a nitrogen-filled and hypoxia-maintaining chamber coupled with a dissolved oxygen analyzer, significant amounts of O_2 were produced by the reaction of MnO_2 (45 μM) with H_2O_2 (100 μM), accompanied by an increase of pH from 6.0 (phosphate/saline buffer, simulating the tumor cells pH) to 8.4 (Figure 4b). These results elucidated that H_2O_2 and H^+ ions could diffuse freely into the reactive sites of the MnO_2 cores in PM NPs, followed by O_2 production and pH increase under hypoxia conditions.

Considering the fact that H_2O_2 is continuously generated in tumor cells, as shown in Figure 4c, we attempted to simulate the *in vivo* conditions by continuously adding H_2O_2 (250 μM) every 30 min with a preliminary concentration of MnO_2 (300 μM). We observed a single dose of the PMB NPs could continuously generate O_2 for five cycles of 30 min. Furthermore, if we conduct the reaction in a smaller vessel, abundant oxygen bubbles were observed, vividly demonstrating the strong capability of MnO_2 to induce H_2O_2 decomposition and O_2 generation (Figure S4).

In addition, we measured the $^1O_2$ generation rate of PMB NPs in aqueous solution by the UV absorbance decrease of DPBF (an indicator of $^1O_2$), as shown in Figure 5. Under 635nm irradiation, the absorbance of DBPF at 425nm decreased sharply every 1 min irradiation, indicating the high efficiency of the generation of singlet oxygen. In addition, there are no obvious subtraction of BODIPY absorbance, implying its outstanding photostability during PDT treatment.

Cancer Cells Uptake and PDT Cytotoxicity of PMB NPs

It is reported that the cancer cellular concentration of H_2O_2 significantly elevated because of the aberrant metabolism.[32] We hypothesized that the PMB NPs could react with endogenous H_2O_2, if they were taken up by cancer cells under hypoxic stress, thus producing O_2 in situ and then acting on PDT. To prove this, the cellular uptake experiments of PMB NPs by human HepG2 and murine 4T1 cells were both carried out. Cancer cells were firstly incubated with nanoparticles for different periods of time, and then observed through fluorescence imaging. As shown in Figure 6, the fluorescence intensity of BODIPY increased obviously over time in the cytoplasm and perinuclear region, which illustrated the endocytosis of the nanoparticles into cancer cells with favorable cytocompatibility (Figure S5).

The cancer cell killing efficacy of PMB NPs in a series of different conditions was then tested. MTT assays against HepG2 and 4T1 cells were conducted at normal or hypoxia atmosphere. Moreover, the effect of MnO_2 against H_2O_2 on PDT efficiency was measured by incubating cells with or without exogenous 100 μM H_2O_2 added for 4h at hypoxia atmosphere.

Generally, a 635nm lamp was used for the irradiation experiments. Cells were irradiated for 10 min with power density of 25 mW/cm², which was extremely low as far as reported. As shown in Figure 7, PMB NPs did not show too much cytotoxicity to cells under dark. However, in normal (5% CO_2) atmosphere, the suppression rates keep gradually increased as the concentration of BODIPY increased when light irradiation was added. At a

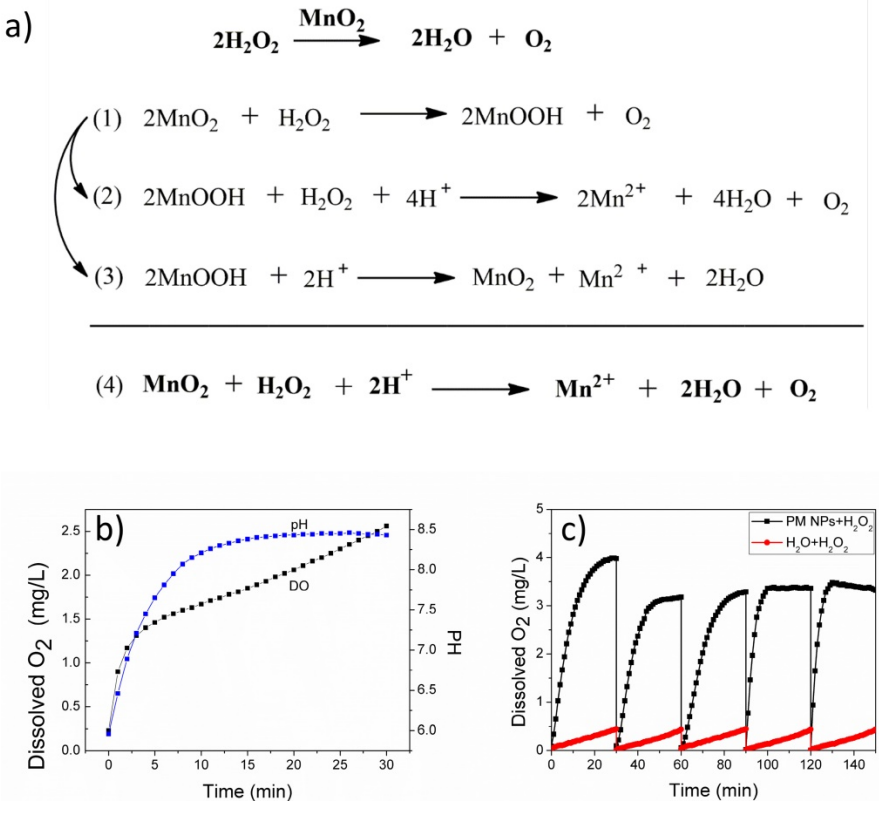

Figure 4. Reactivity of PM NPs toward H_2O_2: (a) Reaction MnO_2 with H_2O_2 to produce O_2 at the presence of H^+; (b) O_2 generation and pH increase by reaction of PM NPs with H_2O_2; (c) O_2 generation by continuous addition of H_2O_2 to PMB NPs solution.

concentration of 12.9 μM, the mortality of the cells increased appreciably with irradiation, 36% HepG2 cells and 43% 4T1 cells dies higher than that incubated under dark.

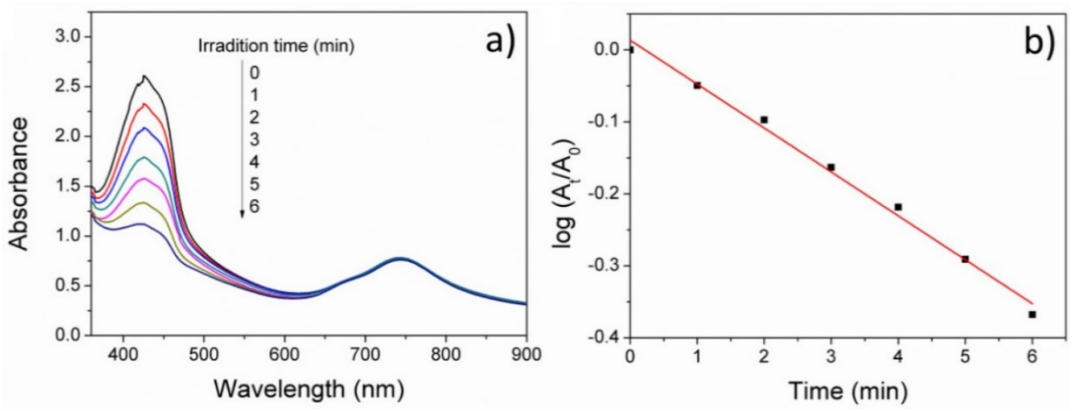

Figure 5. (a) UV-vis absorption spectra of DPBF upon irradiation with PMB NPs in 2% DMSO-water solution under 635nm irradiation, and (b) plots of absorbance decrease of DPBF at 425nm at different irradiation times at room temperature.

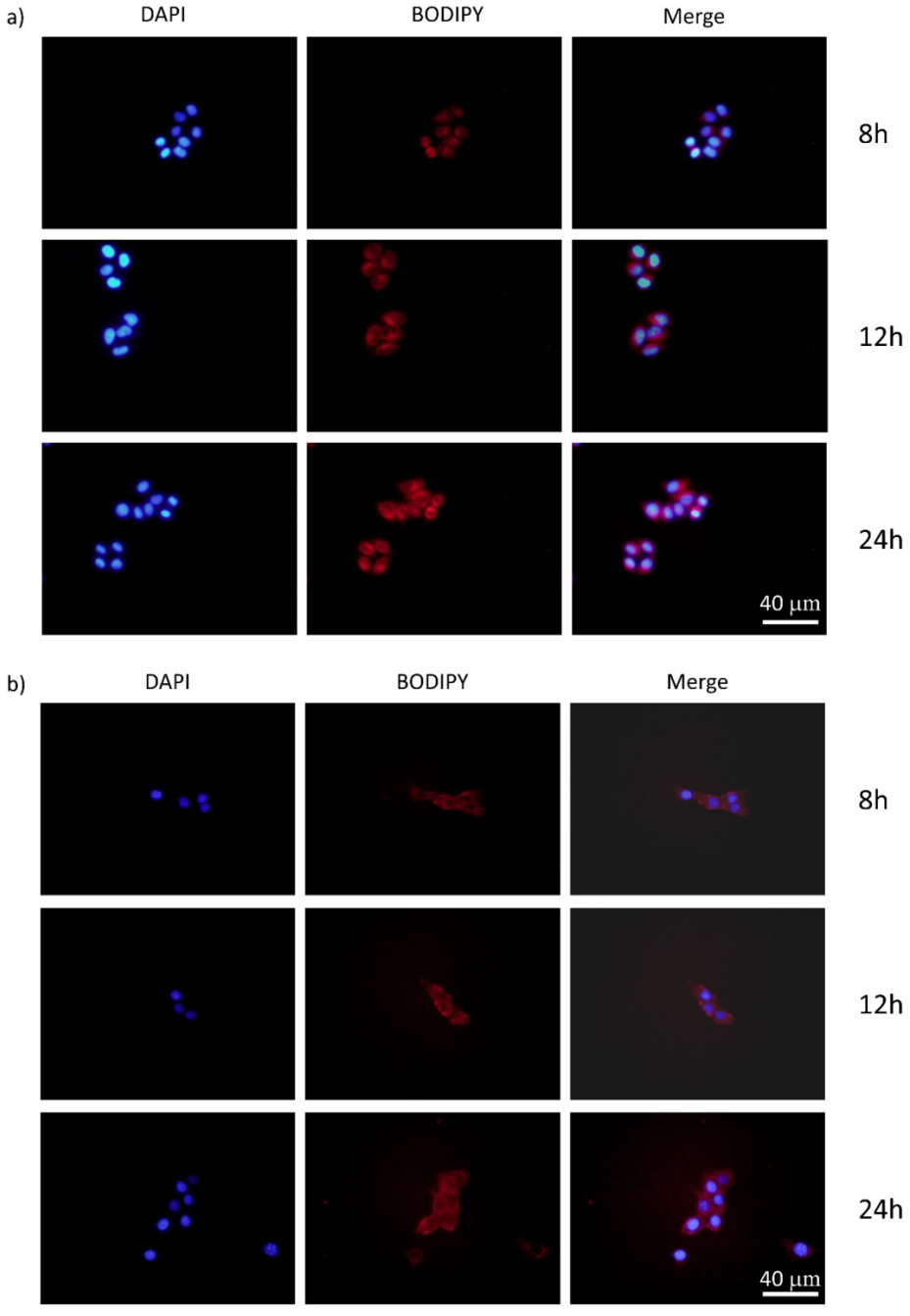

Figure 6. The fluorescence images of (a) HepG2 and (b) 4T1 cancer cells cultured with PMB NPs 8 h, 12 h and 24 h.

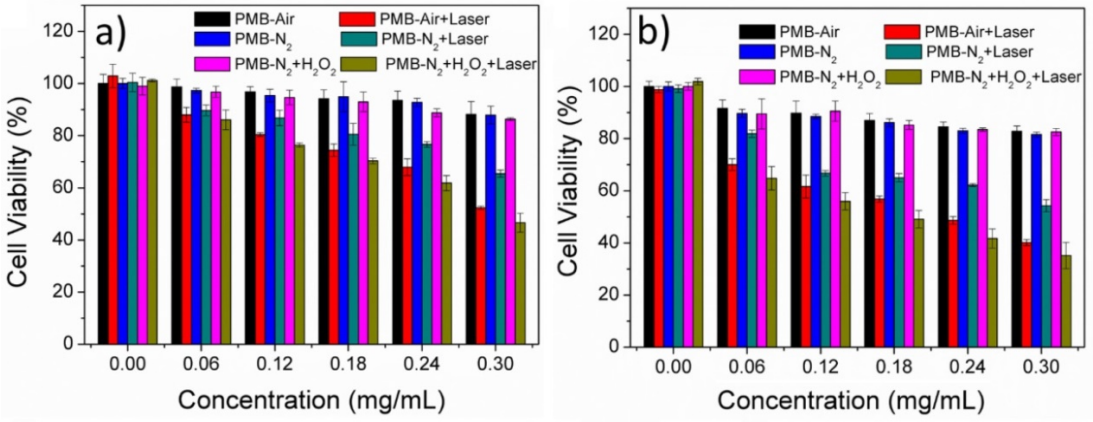

Figure 7. Cytotoxicity of PMB NPs to (a) HepG2 and (b) 4T1 cells with or without irradiation under different conditions.

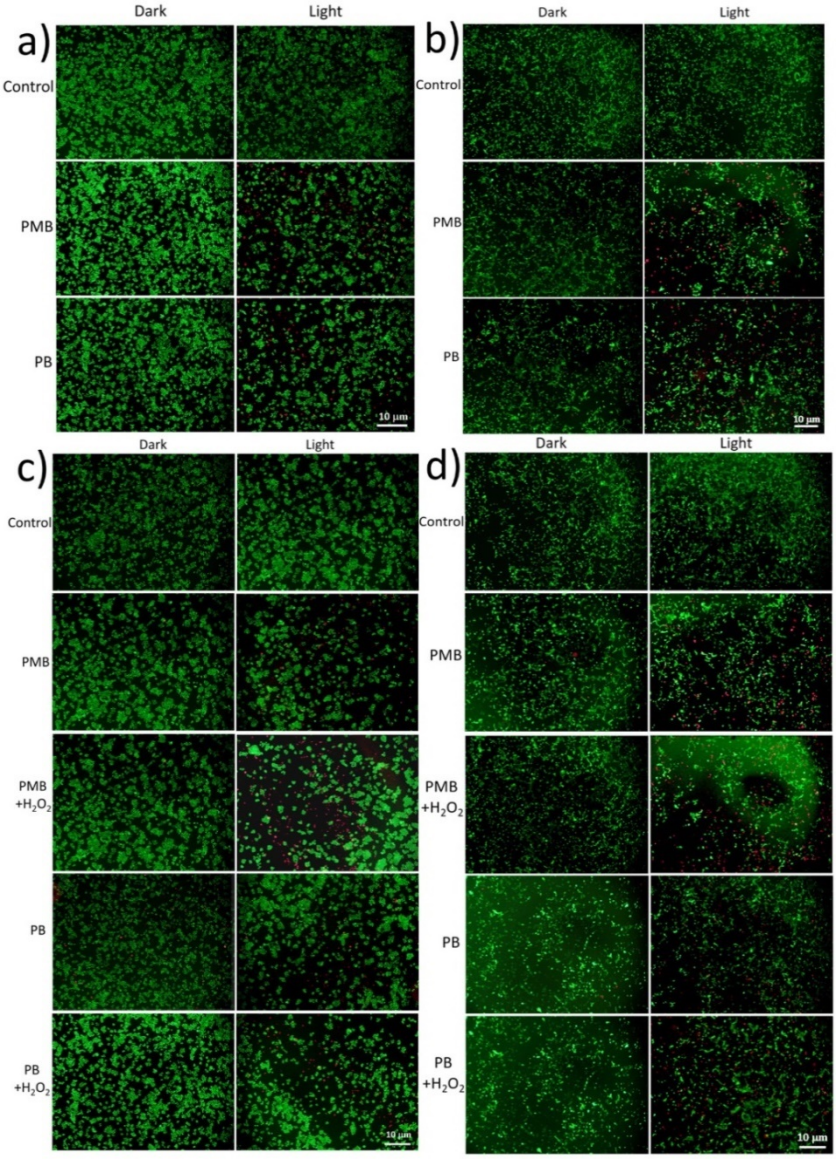

Figure 8. FDA/PI dyed images of cancer cells treated PMB or PB NPs with or without illumination (635nm, 25mW/cm$_2$, 10 min) and H_2O_2: (a) HepG2 and (b) 4T1 cells under normal atmosphere; (c) HepG2 and (d) 4T1 cells under hypoxia atmosphere.

Then, in the nitrogen atmosphere, the added NPs exhibited no distinct dark cytotoxicity to cancer cells with additional H_2O_2 added. However, under light irradiation, the PDT efficiency enhanced obviously (25% suppression rate), especially after the addition of H_2O_2 (upto extra 20% suppression rate increased), nearly similar to the suppression rates with the same BODIPY concentrations incubated in normal atmosphere. At the same time, nanoparticles without MnO_2 (polymer-BODIPY, PB NPs) was also prepared referencing our previous work,[33] and the PDT efficiency of PB NPs was tested in a similar way (Figure S6). Interestingly, we found that the adding exogenous H_2O_2 could only enhance the PDT efficacy of PMB NPs with MnO_2 but not for PB NPs without MnO_2.

In another way to study the PDT effect on cancer cells, imaging of dead (red) and live (green) cells was carried out with propidium iodide (PI) and fluorescein diacetate (FDA) staining. Coincidentally, the FDA/PI dyeing tests conformed to the MTT results perfectly. With no obvious cytotoxicity in dark, the growth of both HepG2 and 4T1 cells was effectively expressed under light irradiation, presenting lower cell density and more dead cells compared to the control groups (Figure 8). More importantly, under hypoxia condition, PMB NPs exhibited satisfactory cytotoxicity with light irradiation and H_2O_2 added. More importantly, we conducted DAPI staining assay against HepG2 cells to observe the cell nucleus transformation in the whole PDT process. With no obvious change in dark, the nuclei of HepG2 cells shrunk 2h after light irradiation compared to the control groups, and

increasing number of nuclei became out of shape over time (Figure 9). These results clearly revealed a light driving and H_2O_2 elevating photodynamic therapy property of the as-prepared PMB NPs.

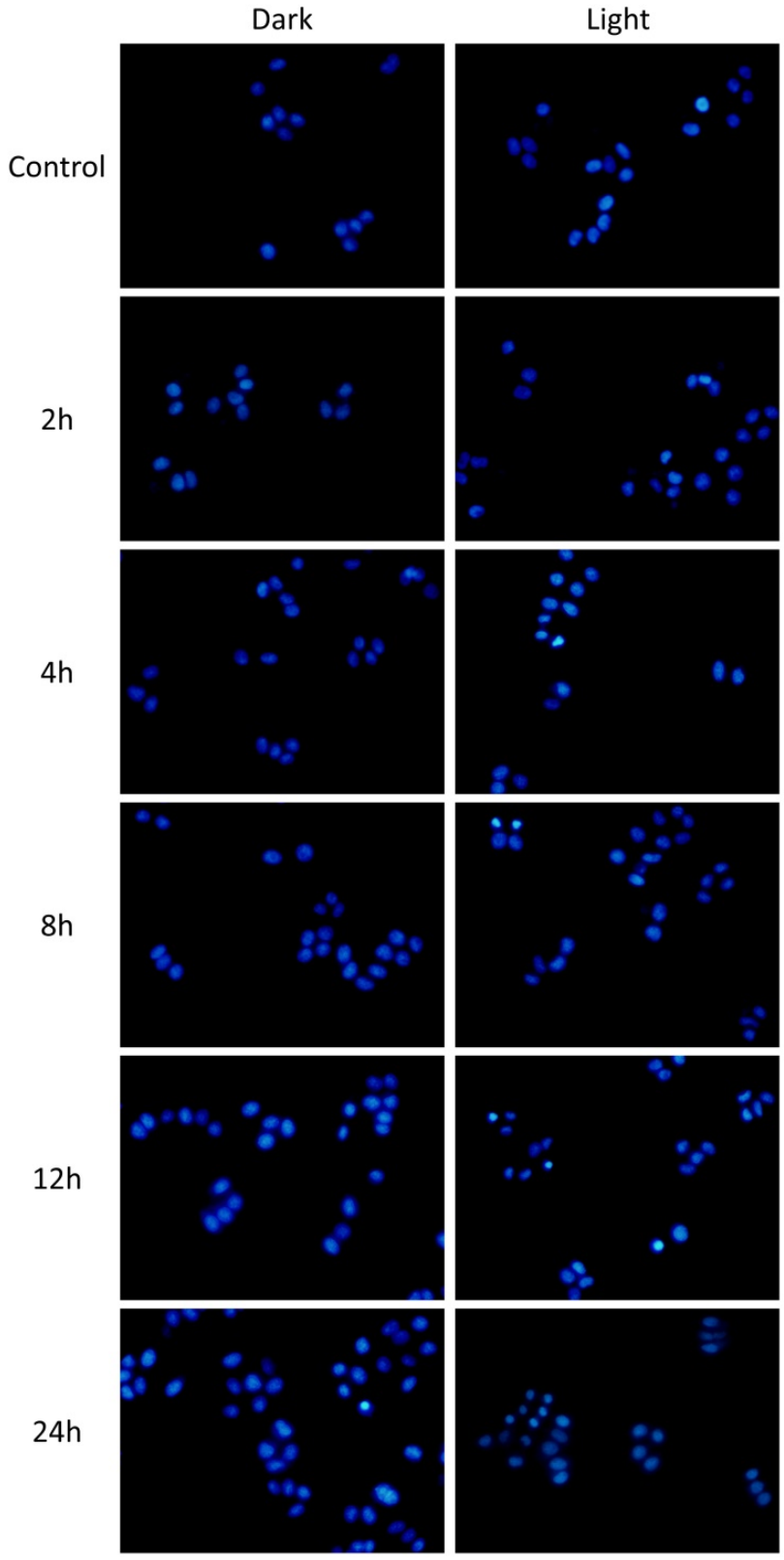

Figure 9. DAPI dyed cell apoptosis images of HepG2 cells treated PMB NPs with or without illumination (635nm, 25mW/cm2, 10 min) under hypoxia atmosphere.

Conclusions

In conclusion, multifunctional H_2O_2 reactive polymer-MnO_2-BODIPY nanoparticles (PMB NPs) were successfully prepared through a simple one-step amino-based reduction reaction followed by emulsion encapsulating method for effective image-guided photodynamic therapy in hypoxia condition. These MnO_2 contained nanoparticles could react with H_2O_2 to produce oxygen so as to overcome hypoxia caused treatment resistance during PDT. Specifically, with an extremely low laser rate, the mortality of the HepG2 and 4T1 cells with light irradiation and H_2O_2 under hypoxia condition increased dramatically compared to cells incubated in the dark, almost catching up with the PDT efficiency in normal condition. Meanwhile, excellent fluorescence property made PMB NPs possible for NIR imaging. All these results highlight the potential of the designed nanoparticles for effective cancer cell tracing and treatment.

Acknowledgment

This work is supported by the National Natural Science Foundation of China (No. 51373162 and 51673180).

Supplementary Material

Scheme of BODIPY synthesis, ^{1}H-NMR of $POEGMA_{30}$ and $PLys_{10}$, optical properties of BODIPY, photo images of PMB solution, and cell tests on HepG2 and 4T1 cancer cells. Supplementary figures.
http://www.ntno.org/v02p0059s1.pdf

Competing Interests

The authors have declared that no competing interest exists.

References

1. Calixto GMF, Bernegossi J, de Freitas LM, Fontana CR, Chorilli M. Nanotechnology-Based Drug Delivery Systems for Photodynamic Therapy of Cancer: A Review. Molecules. 2016; 21:342-8
2. Chan MH, Pan YT, Lee IJ, Chen CW, Chan YC, Hsiao M, et al. Minimizing the Heat Effect of Photodynamic Therapy Based on Inorganic Nanocomposites Mediated by 808 nm Near-Infrared Light. Small. 2017; 13: DOI:10.1002/smll.201700038
3. Gursoy H, Ozcakir-Tomruk C, Tanalp J, Yilmaz S. Photodynamic therapy in dentistry: a literature review. Clin Oral Invest. 2013; 17: 1113-25.
4. Luo T, Zhang QR, Lu QB. Combination of Near Infrared Light-Activated Photodynamic Therapy Mediated by Indocyanine Green with Etoposide to Treat Non-Small-Cell Lung Cancer. Cancers. 2017; 9:63.

5. Qiu KQ, Wang JQ, Song CL, Wang LL, Zhu HY, Huang HY, et al. Crossfire for Two-Photon Photodynamic Therapy with Fluorinated Ruthenium (II) Photosensitizers. Acs Appl Mater Inter. 2017; 9: 18482-92.
6. Kamkaew A, Lim SH, Lee HB, Kiew LV, Chung LY, Burgess K. BODIPY dyes in photodynamic therapy. Chem Soc Rev. 2013; 42: 77-88.
7. Awuah SG, Polreis J, Biradar V, You Y. Singlet Oxygen Generation by Novel NIR BODIPY Dyes. Org Lett. 2011; 13: 3884-7.
8. Choi SY, Baek SH, Chang SJ, Song Y, Rafique R, Lee KT, et al. Synthesis of upconversion nanoparticles conjugated with graphene oxide quantum dots and their use against cancer cell imaging and photodynamic therapy. Biosens Bioelectron. 2017; 93: 267-73.
9. Gao M, Fan F, Li DD, Yu Y, Mao KR, Sun TM, et al. Tumor acidity-activatable TAT targeted nanomedicine for enlarged fluorescence/magnetic resonance imaging-guided photodynamic therapy. Biomaterials. 2017; 133: 165-75.
10. Guo L, Ge JC, Liu Q, Jia QY, Zhang HY, Liu WM, et al. Versatile Polymer Nanoparticles as Two-Photon-Triggered Photosensitizers for Simultaneous Cellular, Deep-Tissue Imaging, and Photodynamic Therapy. Adv Healthc Mater. 2017; 6: 1601431.
11. Kamimura M, Omoto A, Chiu HC, Soga K. Enhanced Red Upconversion Emission of NaYF4:Yb3+, Er3+, Mn2+ Nanoparticles for Near-infrared-induced Photodynamic Therapy and Fluorescence Imaging. Chem Lett. 2017; 46: 1085-7.
12. Zhang PC, Zhang ZH, Jiang XZ, Rui LL, Gao Y, Zhang WA. Unimolecular micelles from POSS-based star-shaped block copolymers for photodynamic therapy. Polymer. 2017; 118: 268-79.
13. An FF, Zhang XH. Pure photosensitizer nanocrystals stabilized with amphiphilic multidentate polymer ligands on the surface for ultra-high payload and enhanced photodynamic therapy. J Control Release. 2013; 172: E29.
14. Castriciano MA, Zagami R, Casaletto MP, Martel B, Trapani M, Romeo A, et al. Poly(carboxylic acid)-Cyclodextrin/Anionic Porphyrin Finished Fabrics as Photosensitizer Releasers for Antimicrobial Photodynamic Therapy. Biomacromolecules. 2017; 18: 1134-44.
15. Li J, Zhang WD, Hu ZJ, Jiang XJ, Ngai T, Lo PC, et al. Novel phthalocyanine and PEG-methacrylates based temperature-responsive polymers for targeted photodynamic therapy. Polym Chem-Uk. 2013; 4: 782-8.
16. Ariffin AB, Forde PF, Jahangeer S, Soden DM, Hinchion J. Releasing Pressure in Tumors: What Do We Know So Far and Where Do We Go from Here ? A Review. Cancer Res. 2014; 74: 2655-62.
17. Broekgaarden M, Weijer R, Krekorian M, van den IJssel B, Kos M, Alles LK, et al. Inhibition of hypoxia-inducible factor 1 with acriflavine sensitizes hypoxic tumor cells to photodynamic therapy with zinc phthalocyanine-encapsulating cationic liposomes. Nano Res. 2016; 9: 1639-62.
18. Luo ZY, Zheng MB, Zhao PF, Chen Z, Siu FM, Gong P, et al. Self-Monitoring Artificial Red Cells with Sufficient Oxygen Supply for Enhanced Photodynamic Therapy. Sci Rep. 2016; 6: 23393.
19. Jung HS, Han J, Shi H, Koo S, Singh H, Kim HJ, et al. Overcoming the Limits of Hypoxia in Photodynamic Therapy: A Carbonic Anhydrase IX-Targeted Approach. J Am Chem Soc. 2017; 139: 7595-602.
20. Liu CP, Wu TH, Liu CY, Chen KC, Chen YX, Chen GS, et al. Self-Supplying O-2 through the Catalase-Like Activity of Gold Nanoclusters for Photodynamic Therapy against Hypoxic Cancer Cells. Small. 2017; 13: 1700278.
21. Cheng YH, Cheng H, Jiang CX, Qiu XF, Wang KK, Huan W, et al. Perfluorocarbon nanoparticles enhance reactive oxygen levels and tumour growth inhibition in photodynamic therapy. Nat Commun. 2015; 6:8785.
22. Chen Q, Feng LZ, Liu JJ, Zhu WW, Dong ZL, Wu YF, et al. Intelligent Albumin-MnO2 Nanoparticles as pH-/H2O2-Responsive Dissociable Nanocarriers to Modulate Tumor Hypoxia for Effective Combination Therapy. Adv Mater. 2016; 28: 7129-32.
23. Jing TT, Fu LY, Liu L, Yan LF. A reduction-responsive polypeptide nanogel encapsulating NIR photosensitizer for imaging guided photodynamic therapy. Polym Chem. 2016; 7: 951-7.
24. Fu LY, Sun CY, Yan LF. Galactose Targeted pH-Responsive Copolymer Conjugated with Near Infrared Fluorescence Probe for Imaging of Intelligent Drug Delivery. Acs Appl Mater Inter. 2015; 7: 2104-15.
25. Prasad P, Gordijo CR, Abbasi AZ, Maeda A, Ip A, Rauth AM, et al. Multifunctional Albumin-MnO2 Nanoparticles Modulate Solid Tumor Microenvironment by Attenuating Hypoxia, Acidosis, Vascular Endothelial Growth Factor and Enhance Radiation Response. Acs Nano. 2014; 8: 3202-12.
26. Gordijo CR, Abbasi AZ, Amini MA, Lip HY, Maeda A, Cai P, et al. Design of Hybrid MnO2-Polymer-Lipid Nanoparticles with Tunable Oxygen Generation Rates and Tumor Accumulation for Cancer Treatment. Adv Funct Mater. 2015; 25: 1858-72.
27. Julien C, Massot M, Rangan S, Lemal M, Guyomard D. Study of structural defects in gamma-MnO2 by Raman spectroscopy. J Raman Spectrosc. 2002; 33: 223-8.
28. Wu SS, Chen WF, Yan LF. Fabrication of a 3D MnO2/graphene hydrogel for high-performance asymmetric supercapacitors. Journal of Materials Chemistry A. 2014; 2: 2765-72.
29. Filatov MA, Karuthedath S, Polestshuk PM, Savoie H, Flanagan KJ, Sy C, et al. Generation of Triplet Excited States via Photoinduced Electron Transfer in meso-anthra-BODIPY: Fluorogenic Response toward Singlet Oxygen in Solution and in Vitro. J Am Chem Soc. 2017; 139: 6282-5.
30. Liu L, Fu LY, Jing TT, Ruan Z, Yang LF. pH-Triggered Polypeptides Nanoparticles for Efficient BODIPY Imaging-Guided Near Infrared Photodynamic Therapy. Acs Appl Mater Inter. 2016; 8: 8980-90.
31. Peng J, Hou XF, Zeng F, Wu SZ. Fluorescent nanoprobe for in-vivo ratiometric imaging of endogenous hydrogen peroxide resulted from drug-induced organ damages. Biosens Bioelectron. 2017; 94: 278-85.
32. Lopez-Lazaro M. Dual role of hydrogen peroxide in cancer: Possible relevance to cancer chemoprevention and therapy. Cancer Lett. 2007; 252: 1-8.
33. Liu L, Ruan Z, Li TW, Yuan P, Yan LF. Near infrared imaging-guided photodynamic therapy under an extremely low energy of light by galactose targeted amphiphilic polypeptide micelle encapsulating BODIPY-Br-2. Biomater Sci. 2016; 4: 1638-45.